Available online at www.sciencedirect.com

Food and Bioproducts Processing

journal homepage: www.elsevier.com/locate/fbp

Effect of reverse osmosis pre-processing of acid whey and electrodialysis current density on process performance

Emilie N. Nielsen[a], *Mathias Gøtke*[a], *Ulysse Cordin*[b], *Leif H. Skibsted*[a], *Svetlozar Velizarov*[c], *João G. Crespo*[c], *Lilia M. Ahrné*[a,*]

[a] *Department of Food Science, University of Copenhagen, Rolighedsvej 26, 1958 Frederiksberg, Denmark*
[b] *Agrocampus OUEST, 65 rue de Saint Brieuc - CS 84215, 35042 Rennes Cedex, France*
[c] *LAQV/REQUIMTE, Department of Chemistry, NOVA School of Science and Technology, FCT NOVA, Universidade NOVA de Lisboa, 2829-516 Caparica, Portugal*

ARTICLE INFO

Article history:
Received 14 October 2022
Received in revised form 26 April 2023
Accepted 5 May 2023
Available online 8 May 2023

Keywords:
Acid whey
Electrodialysis
Lactate
Minerals
Sugars
Separation efficiency

ABSTRACT

Acid whey (AW) is the main side-stream from acidified dairy products, known for its high contents of lactic acid and minerals. The present work investigates the effect of reverse osmosis (RO) pre-processing of AW (ROAW) and the current density during electrodialysis (ED) on the ED process performance. Firstly, the limiting current density of the ED system when treating AW and ROAW was determined. Then, the AW and ROAW have been demineralized and deacidified at under-limiting or over-limiting current density batch operating conditions. RO pre-processing of AW and current density strongly affect the demineralization rate and solutes mass transport across the membranes. Lactate transport can be rationalized by the weak acid dissociation mechanism, while water splitting played a minor role in the ED process performance. Among cations, calcium and magnesium were most affected by RO pre-processing, due to their high affinity to the cation exchange membranes. Lactose and galactose were found in small amounts in the concentrate solution, while no glucose was detected for most conditions even though the glucose content decreased in the diluates. The energy consumption was up to 2 fold higher for ROAW compared to AW

1. Introduction

Acid whey (AW) is the main side stream from a variety of dairy products such as skyr, Greek yoghurt, quark and cottage cheese. The demand for these dairy products is increasing, and so is the generation of AW (Ganju and Gogate, 2017). AW has low concentration of proteins, and therefore cannot be compared with sweet whey, which is the by-product from cheese production based on enzymatic renneting (Carter et al., 2021; Nielsen et al., 2021). Instead, AW is known for its high concentrations of lactose and lactic acid as well as minerals, such as calcium (Nielsen et al., 2021; Nielsen et al., 2022a). The presence of lactic acid and minerals in high concentrations lowers the glass transition temperature and, consequently, the crystallization yield, and thereby hinders the production of a good quality AW powder (Chandrapala and Vasiljevic, 2017; Chandrapala et al., 2016b; Dufton et al., 2019).

* Corresponding author.
E-mail addresses: Emilie.nyborg@food.ku.dk (E.N. Nielsen), mathiasgoetke@gmail.com (M. Gøtke), ulysse1054@gmail.com (U. Cordin), ls@food.ku.dk (L.H. Skibsted), s.velizarov@fct.unl.pt (S. Velizarov), jgc@fct.unl.pt (J.G. Crespo), Lilia@food.ku.dk (L.M. Ahrné).

https://doi.org/10.1016/j.fbp.2023.05.002

The use of electrodialysis (ED) to demineralize and deacidify AW has shown great potential as investigated during the latest years (Beaulieu et al., 2020; Chen et al., 2016; Dufton et al., 2018, 2019; Nielsen et al., 2021). In order to improve the efficiency of the ED treatment, several options have been tested such as different ED operation configurations (Dufton et al., 2018), pre-treatment of the AW with nanofiltration and ultrafiltration (Merkel et al., 2021; Nielsen et al., 2022b; Talebi et al., 2020) and integration of nanofiltration membranes in the ED stack (Beaulieu et al., 2020).

The removal of lactic acid from acid whey, not only increases the value of the produced whey powder (Merkel et al., 2021), but it is also of high interest since lactic acid can be used as an acidulant in other dairy and food products. Deacidification of acid whey is, thus, an essential step during the ED process. Furthermore, following the rate of demineralization of the cations present is also of high importance, as acid whey contains large amounts of calcium, magnesium, potassium and sodium (Menchik et al., 2019; Nielsen et al., 2021), which can precipitate causing scaling and deteriorating the ED performance, as they can bind strongly to the IEM increasing membrane resistance to flow of other ions (Casademont et al., 2008; Dufton et al., 2018; Mikhaylin and Bazinet, 2016). On the other hand, calcium and magnesium transported to the ED concentrate can be used as mineral fortifiers in other food products.

As pointed out in the literature the separation effectiveness of weak inorganic as well as organic electrolytes, such as carboxylic acids, is quite complex and needs thorough understanding to predict their mass transport behavior (Pismenskaya et al., 2001; Chandra et al., 2018; Rybalkina et al., 2022). This is due to their incomplete hydrolysis, which cause relatively low solution conductivity, slower diffusion rates (in case of large weak electrolyte anions) through the AEMs and rise in their resistance. The pH of the depleted solution decreases, while the pH of the enriched (concentrate) solution increases. These processes are intensified when the current becomes close to the limiting one, since, as discussed by Pismenskaya et al. (2002), water dissociation can be catalysed by a weak-acid anion in the AEM to give an acid molecule and an OH^- ion. The rate constant of this proton-transfer reaction is several orders of magnitude higher than that of water dissociation or H^+ and OH^- generation on quaternary ammonium ionogenic groups (Zabolotskii et al., 1988). Since pH variations can affect both the quality of a complex food solution, such as whey, as well as the stability of the AEMs (via degradation of the quaternary ammonium functional group to tertiary amines in presence of OH^- (Ghalloussi et al., 2013), it has been recently demonstrated that the use of high frequency pulsed electric field can have a beneficial effect on membranes lifespan due to a pH stabilization under such conditions (Lemay et al., 2019; Lemay et al., 2020).

Since lactic acid is a weak monoprotic acid, its transport across an AEM is expected to be strongly affected also by its degree of dissociation, which, in turn, depends on its concentration in the solution. Therefore, knowing how the current density affects the ED performance in terms of AW demineralization efficiency and lactate mass transport, is essential to define the most appropriate operating conditions and thereby improve the ED process performance.

Reverse osmosis (RO) is often used to concentrate dairy products such as AW to reduce the water content and thereby the volume ((Christiansen et al., 2022; Suárez and Riera, 2015; Syrios et al., 2011). Rasmussen et al. (2020) have previously investigated the effect of diluting the ED diluate, and found that the initial diluate conductivity had an effect on the demineralization rate, but did not significantly affect the energy consumption. Chandra et al. (2022) have investigated the influence of salt concentration and pH on LCD and transport of organic acids, and concluded that LCD, resistance to ionic transport and concentration polarization across the liquid diffusion boundary layer at the membrane surface are significantly influenced by the molar concentration, size and mobility of the ions. Furthermore, it has previously been shown that the chemical composition of AW strongly affects the demineralization process during ED (Nielsen et al., 2021; Nielsen et al., 2022a). To the best of our knowledge, the effect or concentration of AW by reverse osmosis (ROAW) on ED performance has not been studied.

Thus, the objective of this work is to investigate the effect of reverse osmosis of acid whey and ED current density on process performance, by initiating the ED process at the three possible operating conditions, namely, underlimiting (ULCD), limiting (LCD) and over-limiting (OLCD) current densities. The ED performance was assessed in terms of demineralization efficiency and total energy consumption.

2. Materials and methods

2.1. Acid whey

AW from the production of conventional skyr was provided by Arla Foods amba (Hobro, Denmark). At 20 °C ± 1 the pH of AW was 4.49 ± 0.08 and the conductivity (mS cm^{-1}) 8.43 ± 0.87. More details of the composition can be found on the supplement material Table S1, or in Nielsen et al. (2021).

2.2. Concentration of acid whey by RO

After receiving, a part of the AW was immediately concentrated by RO. 90 L of AW were concentrated by TFC™ HRX™ 2538 HRX-VYV RO membranes, in a spiral wound module (with an effective area of 1.8 m^2) from Koch Membrane Systems (Stafford, UK) using a MMS SW25 pilot filtration plant from MMS AG Membrane Systems (Urdorf, Switzerland). The concentration process took place at 50 °C and the operating applied pressure was 30 bar. The process was stopped when a mass concentration factor (defined as $\frac{m_t}{m_0}$, where m_t is the mass (g/100 g) of dry matter at time t, and m_0 is the initial dry matter mass (g/100 g)) of 2.5 was reached. This concentration was selected as it represents a significant effect on composition of minerals. The AW RO concentrate and remaining AW were stored at –20 °C until further use.

2.3. ED configuration

To conduct the ED experiments, an EDR-Z/10–0.8 ED laboratory unit (MemBrain s.r.o., Stráž pod Ralskem, Czech Republic) was used. The unit was equipped with 10 cell pairs of heterogeneous AM-PES (anion-exchange) and CM-PES (cation-exchange) Ralex® ion-exchange membranes (MemBrain s.r.o., Stráž pod Ralskem, Czech Republic). The 11 cation-exchange and 10 anion-exchange membranes (21 in total) were arranged in an alternated order (CEM-AEM-CEM), and had a total membrane area of 13.44×10^{-2} m^2. The membrane properties can be found in Merkel and Ashrafi

(2019). The electrical potential difference was applied between two Pt coated terminal titanium electrodes. Two Pt wires connected to the two ends of the membrane stack, were used to measure the applied voltage. An ice water bath was used to control the working temperature at 20 °C during the experiments.

2.4. Limiting current density

The limiting current densities (LCD) of the ED systems when demineralizing AW and the RO treated acid whey (ROAW) were determined using the Cowan and Brown method (Cowan and Brown, 1959). In practice, 2 kg AW or ROAW, 0.75 kg tap water and 0.25 kg ≥ 99% Na_2SO_4 (20 g/L) (Merck KGaA, Darmstadt, Germany) were circulated in the ED stack as the diluate, concentrate and electrodes' rinse solutions, respectively (Section 2.5). The voltage was gradually increased from 0 to 35 V by increments of 1 V maintained for 2 min. After each increment the voltage was turned off for 3 min. This time was pre-checked in screening tests and found to be sufficient to equilibrate the membranes. The resulting currents were monitored, and the values of voltage and current were plotted as resistance (U/I) as a function of reciprocal current (1/I). All solutions were circulated at a constant flow rate of 55 L/h each. The pH of the concentrate was adjusted with 1% (v/v) HCl (analytical grade) and kept below 6.5 in order to prevent precipitation of calcium salts (. All tests were made in duplicates and the obtained average values are reported.

2.5. ED operation protocol

In the present study, the demineralization efficiency of AW has been investigated and compared, initiating the ED process at the three possible operating conditions, namely, under-limiting (ULCD), limiting (LCD) and over-limiting (OLCD) current densities. Throughout the experiments, the currents have been kept constant while the voltages increased, leading to progressive change with time of the ULCD operation mode through LCD to OLCD, and from LCD to OLCD.

For the experiments, the same solutions and initial amounts of diluate, concentrate and electrode rinse solutions were used as for the determination of the limiting current density. Furthermore, also the same volumetric flow rates, temperature and concentrate pH values were maintained (Section 2.4.). The ED unit was operated at a constant current density by manually adjusting (increasing) the voltage. The current densities of the experiments started at the LCD conditions were found from the limiting current density tests. The experiments, which started at ULCD were set to 50% of the LCD, while the initial current densities for the experiments performed at OLCD conditions were set up to 40% above the LCD, which was the maximum voltage limit allowed for the ED unit. During the experiments, the pH, conductivity and temperature of the diluate and concentrate were measured in-line by HQ40d multi-meters from Hach (Copenhagen, Denmark). The pH in the concentrate compartment was in the beginning adjusted with a weak HCl solution to maintain pH below 6.5, that otherwise increased due to release of residual OH^--ions from the membranes after the cleaning procedure. This was done to avoid precipitation of calcium salts (Garcia at al. 2018). After approx. 20 min, the pH in the concentrate compartment naturally decreased due to the transport of lactate ions from the diluate to the concentrate. The experiments were stopped when the diluate was 95% demineralized. The demineralization was calculated using Eq. (1).

$$Demineralization \quad (\%) = \frac{\sigma_0 - \sigma_t}{\sigma_0} \times 100\% \tag{1}$$

where σ_0 and σ_t are the conductivities at time zero and time t. The experiments were conducted in randomized order (Table S2).

2.6. Lactic acid, gluconic acid and carbohydrates

The concentrations of lactic acid, gluconic acid, lactose, glucose and galactose were determined using high-performance liquid chromatography (HPLC) and a refractive index detector from Agilent Technologies (Glostrup, Denmark) equipped with an Aminex HPX-87 H column from Bio Rad (Bio Rad Laboratories, CA, USA). For gluconate detection a UV detector was used. A detailed description of the method can be found in Nielsen et al. (2021).

2.7. Minerals quantification

The concentrations of calcium, magnesium, potassium and sodium were quantified using Inductively Coupled Plasma Atomic Optical Emission Spectroscopy (ICP-OES) 5100 system including a SPR 4 auto-sampler from Agilent Technologies (Glostrup, Denmark) in axial view for all elements as described in Chen et al. (2020). For the quantification, standards from Merck KGaA (Darmstadt, Germany) were used. The protocol for digesting the samples can be found in Nielsen et al. (2021).

2.8. Lactate separation efficiency

The lactate (LA) separation efficiency (S) was calculated by Eq. (2) previously described by Li et al. (2022).

$$S = \frac{\frac{C_{LA}^t}{C_{LA}^0} - \frac{C_i^t}{C_i^0}}{\left(1 - \frac{C_{LA}^t}{C_{LA}^0}\right) + \left(1 - \frac{C_i^t}{C_i^0}\right)} \times 100\% \tag{2}$$

where C_{LA}^t and C_{LA}^0 are the lactic acid concentration at time t and time zero, and C_i^t and C_i^0 are the concentration of the reference ion i at time t and time zero.

2.9. Total energy consumption

The energy consumption (EC) was calculated by Eq. (3).

$$EC\left(\frac{Wh}{kg \quad diluate}\right) = \frac{I \times \int_{t=0}^{t=end} U dt}{m_0} \tag{3}$$

where U is the voltage (V), t is the time of ED (h), I is the current (A) and m_0 is the initial mass of the diluate (kg).

The EC was also calculated based on amount of lactic acid obtained in the concentrate compartment following Eq. (4).

$$EC\left(\frac{kWh}{kg \quad lactic \quad acid}\right) = \frac{\frac{I \times \int_{t=0}^{t=end} U dt}{m_{LA}}}{1000} \tag{4}$$

where m_{LA} is the mass of lactic acid obtained in the concentrate (kg).

2.10. Statistics

All data in this present work are presented as average ± standard deviation. One-way pairwise ANOVA between each of the conditions has been used to determine significant differences ($P < 0.05$).

3. Results and discussion

3.1. Limiting current density

The limiting current values of the ED cell when treating AW and ROAW were determined from voltage-current curves, presented in the Fig. 1. For AW, the limiting current intensity value was found to be 0.62 A while for ROAW the obtained value was equal to 0.82 A. This corresponded to LCD values of 9.7 mA/cm^2 and 12.8 mA/cm^2, respectively. (Fig. 2).

3.2. Demineralization and pH

Increasing the current from ULCD to LCD decreased the time for reaching a 95% demineralization by approx. 50% for both AW and ROAW, while increasing the current from LCD to OLCD only decreased the processing time by 20%. Furthermore, the longer processing time of the ULCD experiments were due to the weaker current applied; hence, even a slight increase in current increased the demineralization rate considerably. Simultaneously, the conductivity in the concentrate compartment increased as a consequence of the enhanced ions transport from the diluate. The conductivity increase in the concentrate matches the conductivity decrease in the diluate. The final conductivities in the AW concentrates were 20.6 ± 0.1 mS/cm, 19.9 ± 0.4 mS/cm and 20.2 ± 0.1 mS/cm for initial ULCD, LCD and OLCD conditions, respectively. For ROAW, the conductivity in the concentrate compartments increased to 31.8 ± 0.0 mS/cm, 30.7 ± 0.1 mS/cm and 30.3 ± 0.6 mS/cm for ULCD, LCD and OLCD, respectively. The higher conductivity of the final concentrates compared to the conductivity of the initial diluate solution can be explained by the difference in the volumes of the diluate and concentrate.

The pH of the AW decreased from 4.4 ± 0.0–3.7 ± 0.1, 3.8 ± 0.0 and 3.8 ± 0.0 when treated at ULCD, LCD and OLCD initial operating conditions, respectively. During its demineralization, the pH of the AW was only slightly affected by the increase in current density, when the AW was between

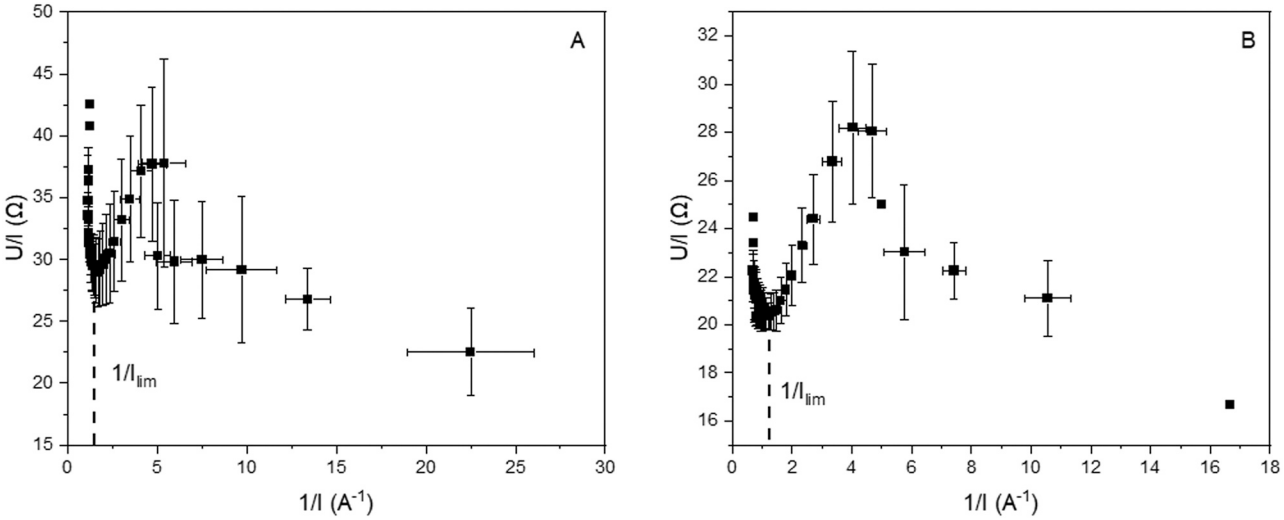

Fig. 1 – Experimental current-voltage curves for the ED cell when treating A) AW and B) ROAW.

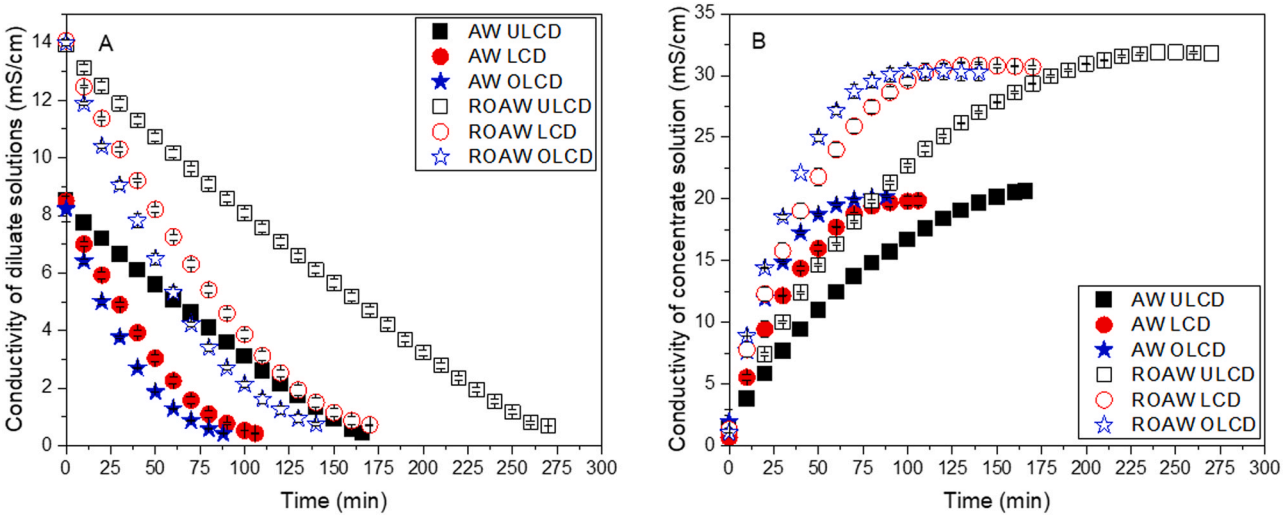

Fig. 2 – Conductivity time evolution in AW and ROAW A) diluate and B) concentrate, at ULCD, LCD and OLCD operating conditions.

65% and 85% demineralized (Fig. 3A). In this demineralization range, the pH was higher at LCD and OLCD. In the ROAW, the pH decreased from 4.4 ± 0.0–3.8 ± 0.0, 4.0 ± 0.0 and 4.1 ± 0.1 applying ULCD, LCD and OLCD, respectively (Fig. 3B). Thus, operating above the LCD resulted in a smaller pH drop than operating below LCD. This is opposite to the findings of Beaulieu et al. (2020), who observed a larger pH drop in AW when using a current density above LCD. They explained the pH drop by the generation of H^+ ions from water splitting. However, as explained by Rybalkina et al. (2022) water splitting is one of the two mechanisms of this generation, occurring at OLCD conditions, while by the second mechanism, H^+ ions are generated during a weak acid dissociation at the depleted diluate solution/anion-exchange membrane interface, while the weak acid anions enter the AEM interior. When leaving the AEM into the adjacent concentrate solution, reestablishment of the equilibrium occurs, which determines their back protonation. The result of this process is the generation of OH^- ions at the membrane/concentrate solution boundary. As it has been reported by Cifuentes-Araya et al. (2011) a combination of fouling of the CEM and a constant current regime can also cause leakage of OH^- ions through the CEM towards the anode and their transport into the diluate, when the current density has reached LCD. More fouling was also found on the CEM used for ROAW than for AW, which support this explanation. Since no water splitting is taking place at ULCD, the pH drop in the diluate of both AW and ROAW using ULCD can be explained by dissociation of lactic acid to lactate and protons. This is a consequence of the shift in the lactic acid/lactate equilibrium, when lactate is removed from the diluate during ED (Chen et al., 2016; Nielsen et al., 2021). The final pH in the concentrate compartment was 4.6 ± 0.1 in all ED experiments (Figs. 3C and 3D).

3.3. *Lactic acid transport*

The lactic acid concentration decreased in the AW from initially 80.0 ± 2.6 mM to 9.2 ± 0.5 mM, 9.2 ± 3.0 mM and 6.7 ± 0.5 mM at the end of ED process when applying ULCD, LCD and OLCD conditions (Fig. 4A), respectively. Thus, the final lactic acid concentration is statistically significantly lower ($P < 0.05$) in the AW when using OLCD compared to ULCD. This can be explained by the depletion of the lactic acid at the diluate solution/anion-exchange membrane interface due to concentration polarization leading to a higher degree of its dissociation according to Ostwald's law of dilution. Also, the co-ion exclusion of the protons increases with the solution dilution, consequently, the possibility of their permeation (co-ion "leakage") across the AEM becomes

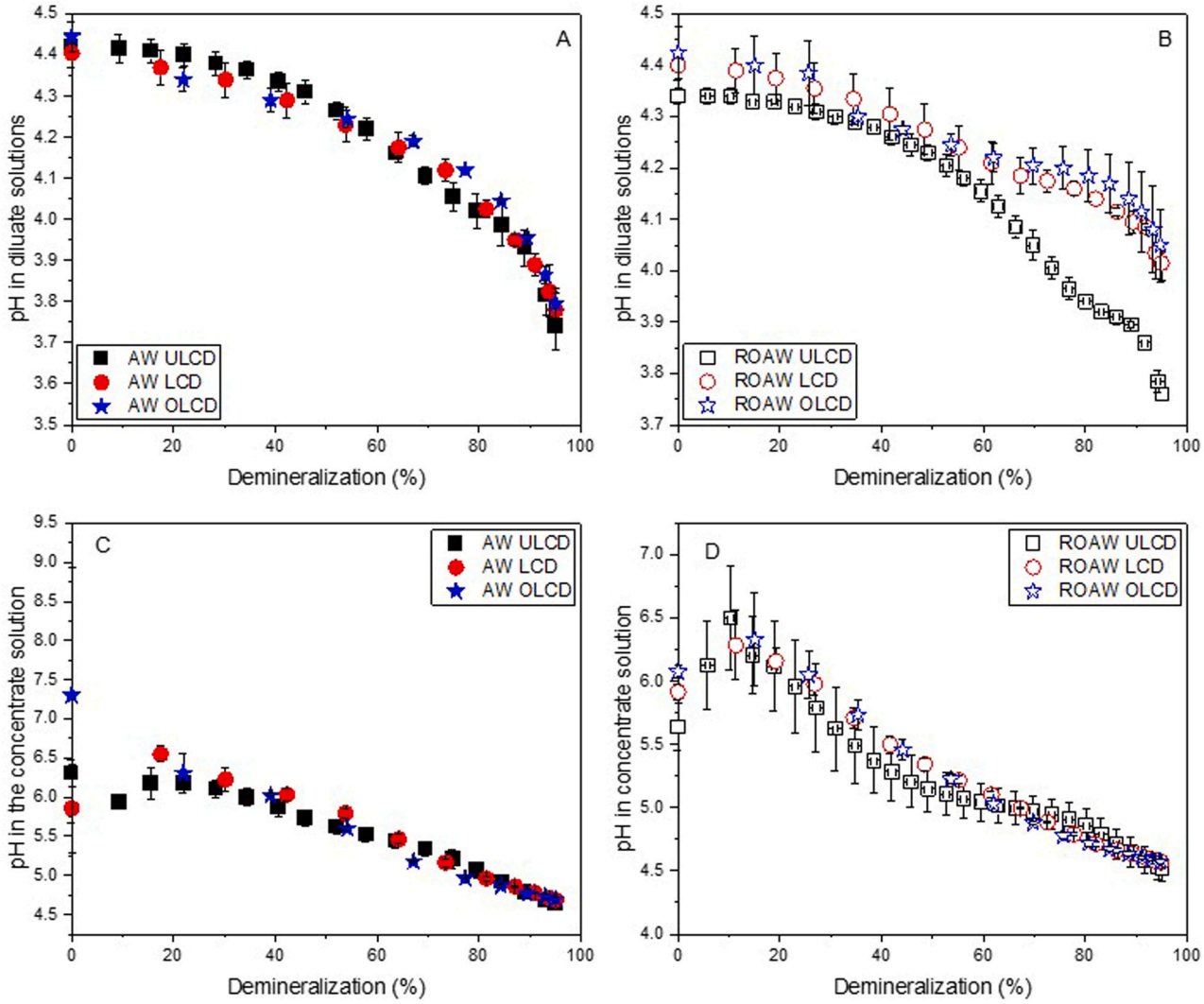

Fig. 3 – pH evolution in A) AW diluate and B) ROAW diluate, C) AW concentrate and D) ROAW concentrate up to a 95% demineralization.

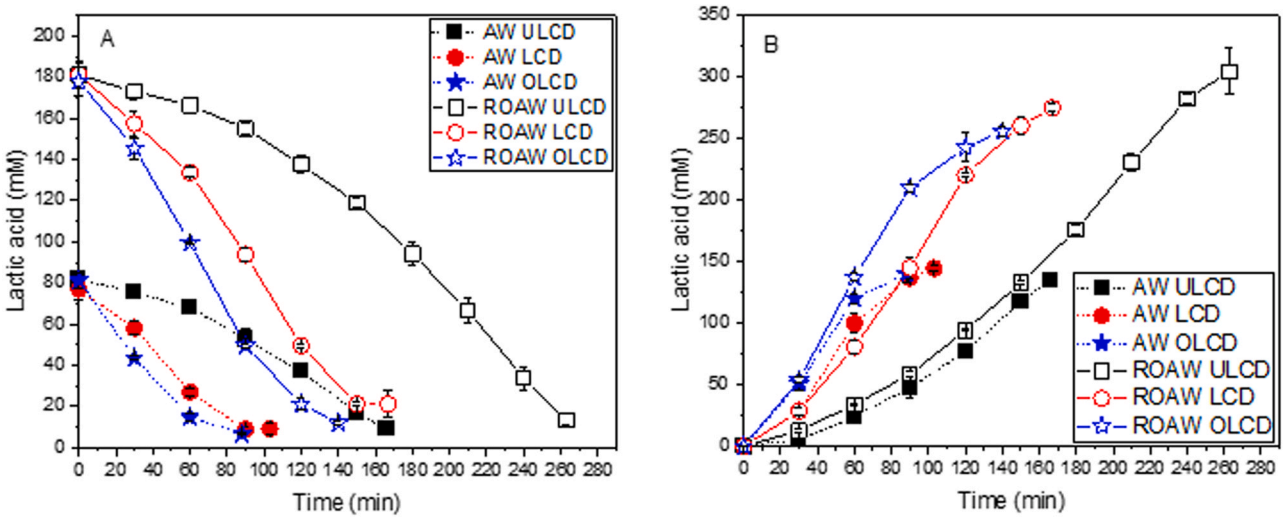

Fig. 4 – Lactic acid concentration time evolution in AW/ROAW in A) diluate and B) concentrate, under ULCD, LCD and OLCD conditions.

much lower. This also affected the ED processing time, for which 80% of lactic acid were removed. For ULCD, 80% of the lactic acid was removed after 151 min, while it only took 78 min and 58 min for LCD and OLCD, respectively.

For the ROAW, the concentration of lactic acid in the diluate decreased from 180.1 ± 1.8 mM to 13.6 ± 2.8 mM, 21.2 ± 6.5 mM and 12.0 ± 0.9 mM for ULCD, LCD and OLCD, respectively. These results indicate that an increase in current density affect less the amount of transported lactate for ROAW compared to the case of AW. However, again the time for reaching 80% lactic acid removal decreased significantly by increasing the current density. 80% of the lactic acid was removed after 239 min starting the ED process at ULCD, 132 min at LCD and 104 min at OLCD. Thus, increasing the current density from ULCD to LCD reduced the time for removing 80% of the lactic acid by 45% and a further increase to OLCD operating conditions reduced the time by 92%. Considering the concentrate compartment, there is a ~ 30 min lag period required for lactate to appear under ULCD initial operating conditions (Fig. 4B). This can be explained by the time needed to approach first the LCD and then the OLCD operating conditions, under which the lactic acid at the AEM side facing the depleted diffusion boundary layer becomes strongly diluted, thus increasing its degree of dissociation Therefore the final lactic acid concentration in the AW concentrate was only affected by the increase in current density from ULCD to LCD, where the final lactic acid concentrations were 134.9 ± 4.8 mM and 144.6 ± 1.8 mM, respectively. For the ROAW the final concentrations of lactic acid in the concentrates were 304.6 ± 19.0 mM, 274.8 ± 3.2 mM and 255.9 ± 3.5 mM for ULCD, LCD and OLCD initial operating conditions, respectively. Interestingly, the lactic acid concentration was lowest in the ROAW concentrate when applying OLCD, even though it decreased most in the ROAW diluate at this current density. The lactic acid must therefore had remained trapped in the AEM as fouling, which is more likely to occur when its concentration in the diluate solution is high (Guo et al., 2014; Lindstrand et al., 2000). This was experimentally confirmed by analysis of the fouled AEM, which showed that 35–100% more lactic acid was found as fouling when the membranes had been used in ROAW compared to AW electrodialysis experiments.

3.4. *Cations transport*

The mass transport rates of cations (calcium, magnesium, sodium and potassium) were highly affected by the applied current density (Fig. 5). As it can be seen, the demineralization rate of the cations increases when the current density increases, which can be clearly associated by the increased electric potential driving force (Beaulieu et al., 2020). However, the final concentrations of the cations in the diluate were generally insignificantly affected by the current density. Only the increase from LCD to OLCD had a significant effect on potassium in ROAW, where the final potassium concentration was 3.1 ± 0.3 mM and 0.5 ± 0.7 mM, respectively. The calcium and magnesium levels were most affected by the increase in their concentrations in ROAW. It is evident that the slope of calcium concentration decrease in the diluate for ULCD becomes steeper when demineralizing ROAW compared to demineralizing AW. The same applies to magnesium. This can be explained by the higher divalent ions affinity to the cation exchange membranes at ULCD, which increases their transport rate (Dufton et al., 2020). The impact is further enhanced, when the concentration of monovalent ions decreased (a reduced competition for the fixed membrane charge sites), which explains the bended shape of the calcium and magnesium curves. This effect is less pronounced at higher current densities. Instead, at higher current densities, the transport of monovalent ions is favored due to their higher diffusivity in solution (Beaulieu et al., 2020; Kim et al., 2012). The time for reaching 80% demineralization for each of the cations is summarized in Table 1. As it can be seen, the transport rate of each cation is affected by the increase in current density. For all conditions, the cations were removed in the following order: $K^+ > Na^+ > Ca^{2+}$ and Mg^{2+}. This order follows the expected trend, defined by the respective decreasing cation diffusion coefficients in water and is in line with previous findings (Chen et al., 2016; Nielsen et al., 2021; Rasmussen et al., 2020).

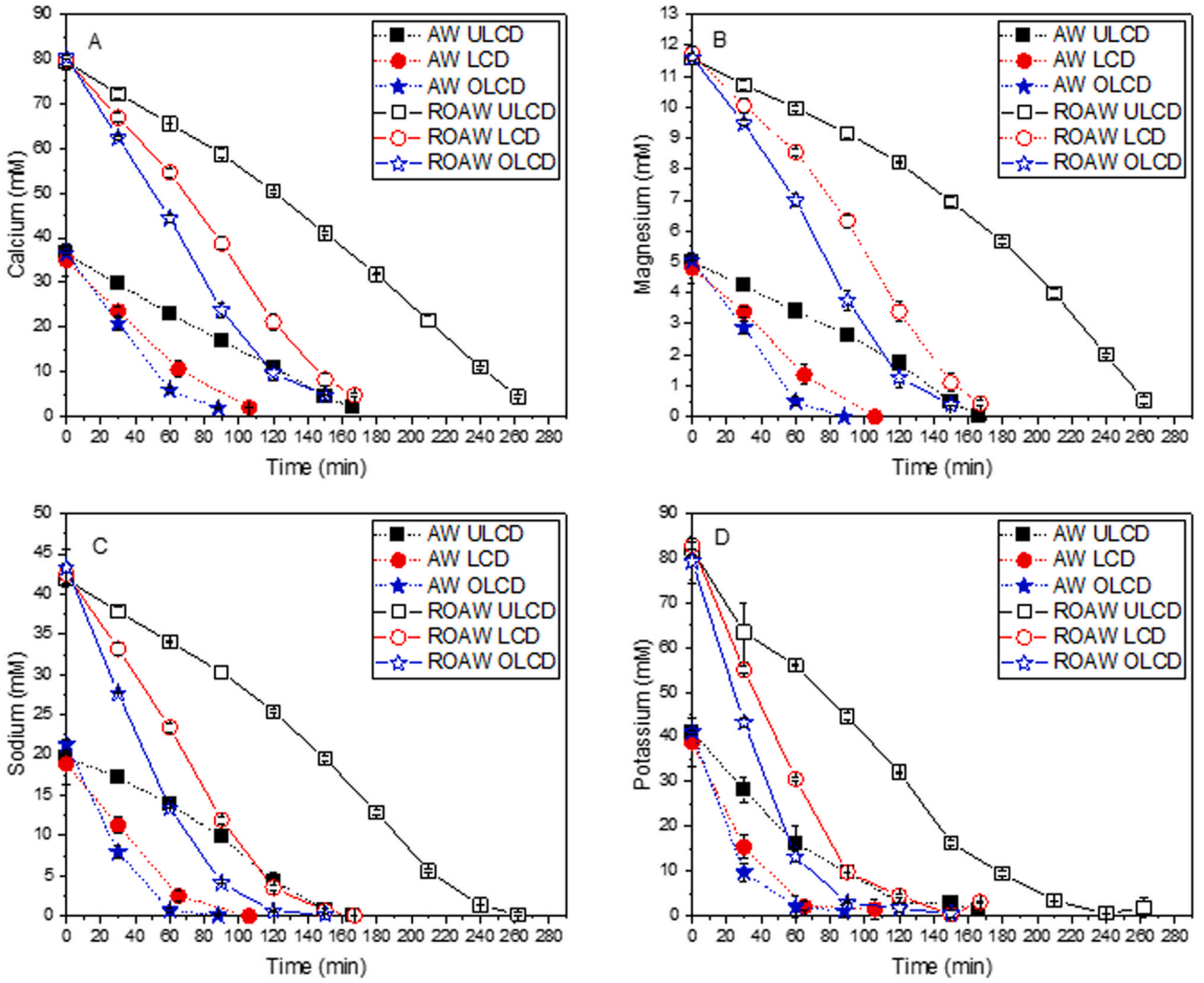

Fig. 5 – Time evolution of A) calcium, B) magnesium, C) sodium, and D) potassium, in AW and ROAW diluates during ED processing.

In Fig. 6, it can be seen that the concentrations of the cations in the concentrate solution increase was slowest when ULCD initial operating conditions were applied. This can be attributed to the lower electrical potential driving force and was most pronounced during the first 60 min for AW and 120 min for ROAW. For the ROAW concentrate it is evident that the concentration of monovalent ions increases faster than the divalent ions, which can be explained by their higher diffusion coefficients and mobility. The final concentrations of calcium in the AW ED concentrates were 69.3 ± 1.4 mM, 60.1 ± 1.0 mM and 59.0 ± 2.3 mM for ULCD, LCD and OLCD, respectively. For magnesium, the final concentrations were 10.3 ± 0.1 mM, 9.2 ± 0.3 mM and 9.1 ± 0.4 mM for ULCD, LCD and OLCD, respectively. The final concentrations of divalent ions are thus higher at lower current density. The same was observed for ROAW, but was most pronounced for calcium, which final concentrations were 141.9 ± 7.6 mM, 126.7 ± 0.5 mM and 118.5 ± 8.7 mM and for the concentrations of magnesium, equal to 18.0 ± 0.6 mM, 17.7 ± 0.4 mM and 17.4 ± 0.9 mM for ULCD, LCD and OLCD, respectively. This confirms that the divalent ions transport was favored at ULCD, and that this behavior cannot be observed at higher current densities because of concentration polarization effects, leading to increased

Table 1 – Time in minutes for reaching 80% removal of each cation from the diluates for AW and ROAW, applying ULCD, LCD and OLCD initial operating conditions.

	Ca^{2+}	Mg^{2+}	Na^{+}	K^{+}
AW ULCD	137.5 ± 2.1[a]	137.5 ± 2.1[a]	124 ± 5.7[a]	96 ± 0[a]
AW LCD	79.5 ± 10.6[b]	74.5 ± 10.6[b]	58 ± 4.2[b]	45.5 ± 0.7[b]
AW OLCD	56.5 ± 2.1[c]	52 ± 2.8[c]	42.5 ± 2.1[c]	33 ± 4.2[c]
ROAW ULCD	225.5 ± 0.7[d]	235 ± 0[d]	198 ± 0[d]	150 ± 0[d]
ROAW LCD	131.5 ± 2.1[e]	132 ± 3.5[a]	101 ± 0[e]	78 ± 0[e]
ROAW OLCD	105 ± 4.2[f]	105 ± 4.3[e]	72.5 ± 2.1[f]	56.5 ± 3.5[f]

[a-f], different letter in column indicates significant difference ($P < 0.05$).

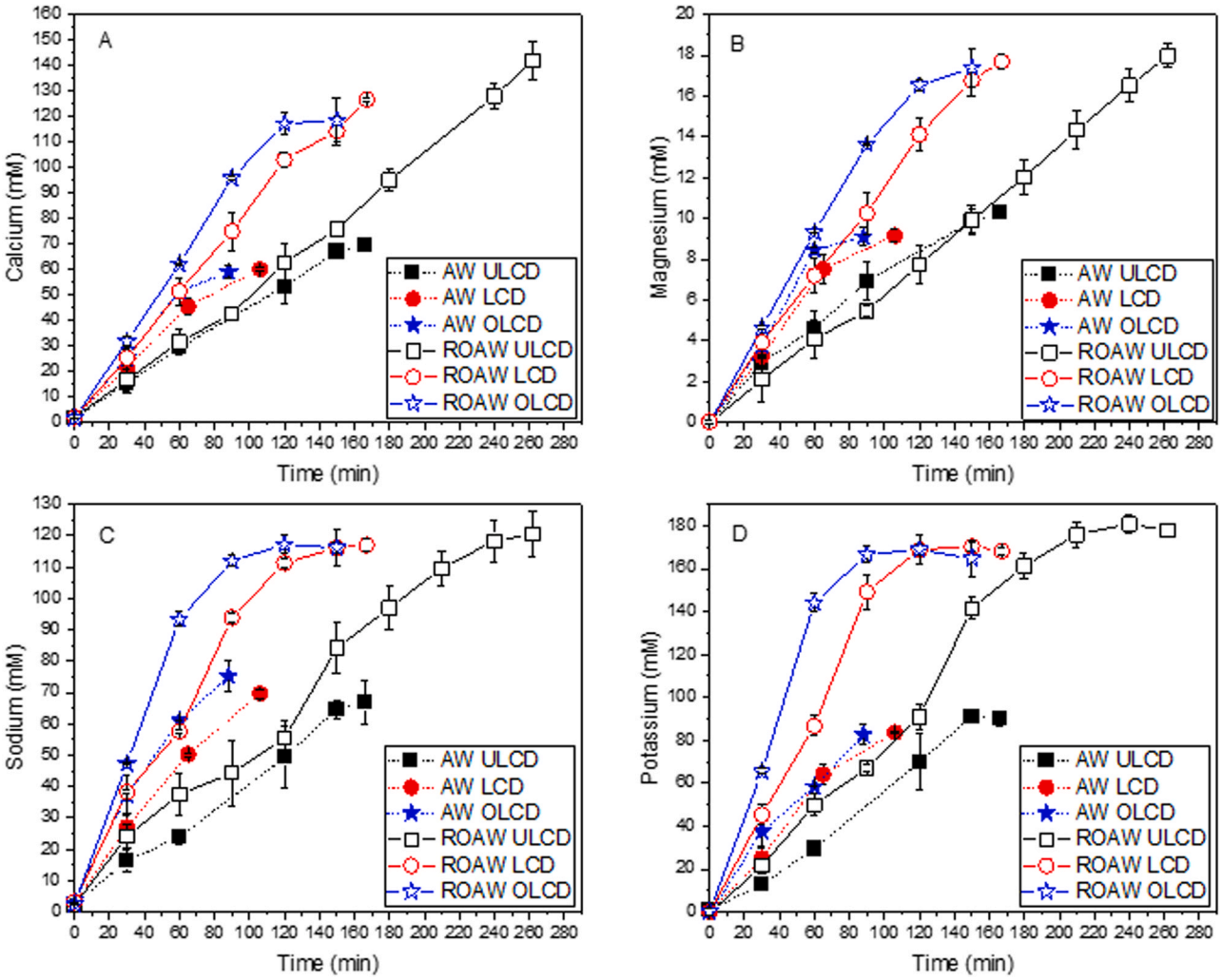

Fig. 6 – Evolution of A) calcium, B) magnesium, C) sodium, and D) potassium, in AW and ROAW concentrates during ED processing.

migration of monovalent ions because of their higher diffusivity in the cation-exchange membrane's liquid diffusion boundary layer interface (Beaulieu et al., 2020; Dufton et al., 2020; Kim et al., 2012).

The final concentrations of sodium in the AW ED concentrates were 66.9 ± 6.7 mM, 69.7 ± 1.5 and 75.2 ± 5.1 mM for ULCD, LCD and OLCD, respectively. There is a tendency for an increasing sodium concentration with an increasing current density, which corresponds to the sodium concentration decrease observed in the diluate when the current density increases. No significant differences were found in the ROAW ED concentrate (120.5 ± 7.2 mM, 117.0 ± 1.9 mM and 116.1 ± 6.0 mM for ULCD, LCD and OLCD, respectively). The concentration of potassium in the AW ED concentrate was found to be 90.3 ± 3.3 mM, 83.7 ± 0.8 mM and 82.6 ± 4.6 mM for ULCD, LCD and OLCD, meaning that a significant decrease in potassium concentration was only found when increasing the current density from ULCD to LCD. The same was observed for ROAW, for which the potassium concentrations were found to be 177.8 ± 3.2 mM, 168.3 ± 1.8 mM and 164.7 ± 8.2 mM under ULCD, LCD and OLCD operating conditions, respectively.

At OLCD operating conditions, the migration of divalent cations was significantly affected by scaling formation, which was experimentally confirmed (Nielsen et al., 2023). Water splitting produces OH^- ions, which increases the pH that, as has been extensively reported in the literature causes formation of precipitates of carbonates and hydroxides of calcium and/or magnesium (Shaposhnik et al., 2002; Atamanenko et al., 2004; Andreeva et al., 2018). The team of Bazinet has comprehensively investigated the mechanisms of these mineral membrane fouling related phenomena and has proposed an efficient way of scaling mitigation by a pulsed electric field (PEF) application (Cifuentes-Araya et al., 2011; Cifuentes-Araya et al., 2012; Cifuentes-Araya et al., 2013; Cifuentes-Araya et al., 2014; Mikhaylin et al., 2014; Mikhaylin et al., 2016).

3.5. *Sugars migration*

During the ED experiments, the concentrations of lactose in the AW changed from 119.1 ± 7.1 mM to 130.1 ± 8.0 mM, 108.4 ± 16.7 mM and 118.5 ± 3.8 mM when applying ULCD, LCD and OLCD operating conditions (Fig. 7A), respectively. The changes were not significant ($P < 0.05$). The lactose concentration in the ROAW increased from 277.2 ± 5.4 mM to 299.0 ± 12.6 mM, 314.5 ± 6.5 mM and 277.6 ± 1.9 mM at ULCD, LCD and OLCD, respectively. The increase in lactose concentration could be explained by the volume reduction of the diluate during the ED process, due to (electro)osmotic water transport to the concentrate. An increase in lactose concentration was also observed in the ED concentrates

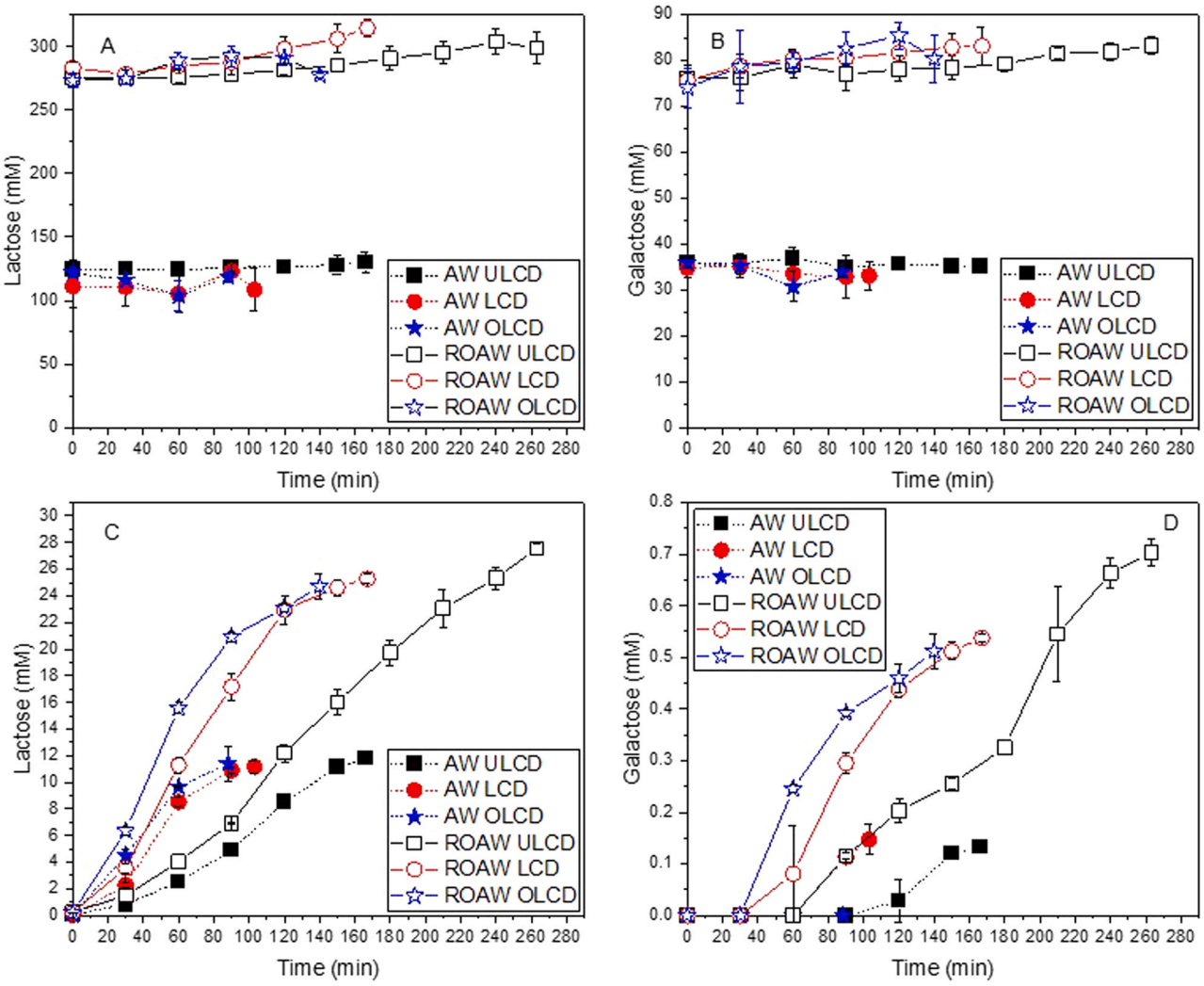

Fig. 7 – Evolution of A) lactose and B) galactose in the ED diluates and C) lactose and D) galactose in the ED concentrates for AW and ROAW when using ULCD, LCD and OLCD operating conditions.

(Fig. 7C). Lactose is a neutral compound not affected by electric field, but can be transported by diffusion due to its concentration gradient across the membranes (Chandrapala et al., 2016a; Lee et al., 2014). For the AW, the final lactose concentration in the ED concentrates was the same and not affected by the applied current density. For the ROAW, the final lactose concentration was slightly higher in the ED concentrate when using ULCD. However, this is presumably due to the longer processing time at this current density, giving more time to lactose diffusion through the ion exchange membranes. Previous studies by Beaulieu et al. (2020) and Chen et al. (2016) report that no or only limited amounts of lactose permeate the ion exchange membranes during ED of acid whey. In both studies, Neosepta ion exchange membranes from Astom (Japan) were used. This indicates that the Ralex® ion exchange membranes are more permeable to lactose than the ion exchange membranes used in the referred study, which is due to the fact that they are heterogenous membranes with more open polymeric structure, while the Neosepta membranes are homogenous and much denser. The same tendency applies for galactose (Figs. 7B and 7D); however, the final galactose concentration in the ED concentrates was much lower, and in some cases not detectable. The low galactose concentration is also reflected in the shape of the curves, in which an initial lag-time can be observed for all conditions, which can be explained by the galactose concentration being below the detection limit of the analytical method used. Furthermore, it is valuable to notice the similarity between the shape of the lactose and galactose curves. However, the slope of increment is higher for galactose than for lactose which makes sense, since galactose is a mono-sugar and thereby is expected to permeate the membranes more easily.

The concentration of glucose decreased in the diluate during the ED processing (Fig. 8A). Data for glucose concentration in AW OLCD diluate is missing. Glucose is also a neutral compound transported by diffusion, as lactose and galactose (Lee et al., 2014). However, for most conditions, it has not been possible to detect glucose in the ED concentrates (Fig. 8B). An explanation for this could be that glucose is oxidized to gluconate by the high voltage applied to the ED system. It is well known that glucose can be electrochemically oxidized to gluconolactone, which hydrolyse to gluconate depending on pH (Beden et al., 1996; Pasta et al., 2010). To confirm this, initial samples of the diluates and final samples of the concentrates have been analysed by HPLC to detect possible presence of gluconate. It was found that gluconate is present in the concentrates after the ED

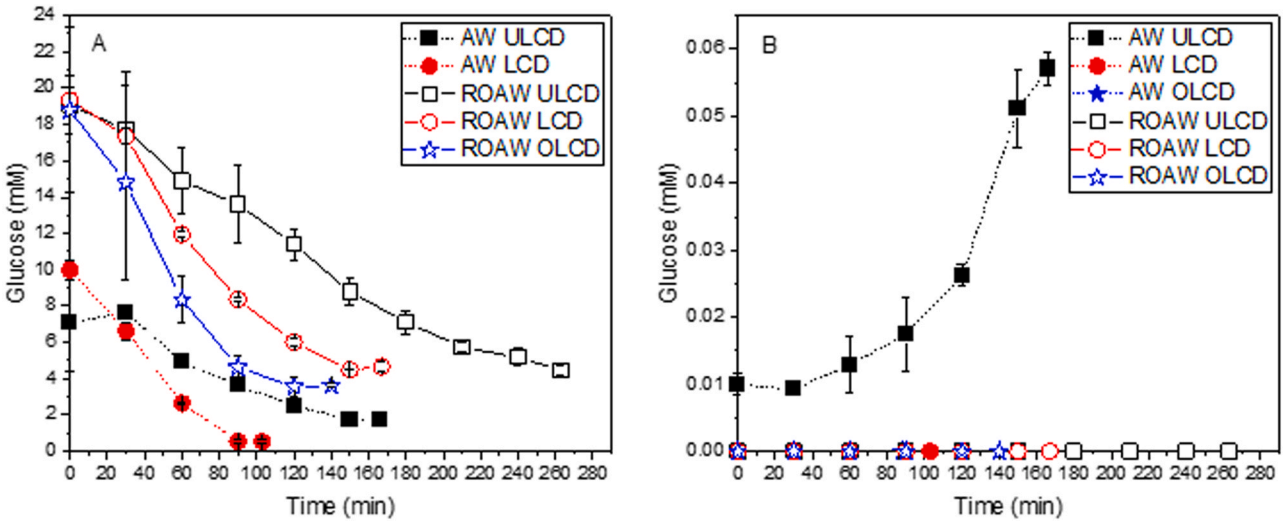

Fig. 8 – Evolution of glucose in ED A) diluate and B) concentrate for AW and ROAW using ULCD, LCD and OLCD operating conditions.

Table 2 – Separation efficiency of lactate during the first and second hour of the ED process.

		Lactate separation efficiency (%)			
		LA^-/Ca^{2+}	LA^-/Mg^{2+}	LA^-/Na^+	LA^-/K^+
1 h	**AW ULCD**	31.5	25.5	22.5	50.3
	AW LCD	3.3	4.8	13.6	17.5
	AW OLCD	11.8	4.7	8.0	7.1
	ROAW ULCD	26.4	18.1	28.8	47.7
	ROAW LCD	7.8	1.3	23.1	37.2
	ROAW OLCD	0.7	0	20.4	28.6
2 h	**AW ULCD**	19.1	14.5	26.5	37.1
	AW LCD	-	-	-	-
	AW OLCD	-	-	-	-
	ROAW ULCD	26.8	12.8	30.8	51.9
	ROAW LCD	0.8	0.0	18.7	20.9
	ROAW OLCD	0	1.0	9.7	9.0

process, while its presence was very limited in the initial samples taken from the diluate. This conclusion is supported by the fact that glucose is only found in the AW using ULCD.

3.6. *Lactate separation efficiency*

For all tested conditions, the lactate separation efficiency was highest when the lactic acid concentration was compared to the potassium concentration (Table 2). This can be explained by potassium being the ion with the highest permeability among the tested ions. In contrast, the lactate separation efficiency is lowest when lactic acid is compared with calcium and magnesium due to their lower permeability coefficients. An increase in applied current density, and thereby increased transport driving force, decreases the lactate separation efficiency. This means that the increased driving force enhances the transport on lactate more than on the other ions, since lactate is squeezing the transmission of the other ions at these current densities (Li et al., 2022). The difference between the lactate separation efficiency during the first and second hour is less pronounced for sodium and potassium compared to calcium and magnesium, and, in some cases, the lactate separation efficiency even increases during the second hour. This could be explained by the higher transfer of sodium and potassium during the second hour due to their higher mobility.

3.7. *Energy consumption*

As expected, the specific energy consumption of the ED processes per kg diluate increased with increasing current density and increasing concentration of the diluate as seen in Table 3. In the calculations only the energy consumption for applying the voltage is taken into account not including the energy demand for pumping the working solutions, which was maintained equal for all tested operating conditions. Beaulieu et al. (2020) have also previously reported increased energy consumptions at increased current densities. At ULCD, the energy consumption increased 1.2-fold from using AW to ROAW. At OLCD, the energy consumption increased 2.0-fold. The mass concentration ratio of the

Table 3 – Energy consumption for applying the voltage for reaching 95% demineralization of AW and ROAW using ULCD, LCD and OLCD.

	AW	ROAW	AW	ROAW
	(Wh/kg diluate)		(kWh/kg lactic acid recovered)	
ULCD	6.83 ± 0.05	8.07 ± 0.20	2.35 ± 0.02	1.71 ± 0.04
LCD	15.72 ± 0.35	33.81 ± 0.91	4.24 ± 0.09	5.60 ± 0.15
OLCD	24.12 ± 0.01	47.90 ± 2.43	6.23 ± 0.00	7.92 ± 0.40

ROAW was equal to 2.5, and, thus, the energy was more efficiently spent on transporting the ions for the ROAW compared to the case of AW. This conclusion is supported by the energy consumption per kg lactic acid recovered in the concentrate compartment. For ULCD, the energy consumption was lowest per kg lactic acid recovered when ROAW was used. For LCD and OLCD the energy consumption was higher for ROAW than AW but only 1.3-fold. However, the RO pre-processing of the acid whey also requires energy, which needs to be accounted for to make a fair comparison of the ED and RO+ED processes.

4. Conclusions

The present study elucidates the effect of RO pre-processing and applied current density during ED processing of AW. It was found that both the RO pre-processing of AW and the applied current density strongly affect the ED performance. It was expressed by: decreased processing time at higher current densities, longer processing time for demineralization of ROAW compared to AW, lower lactate separation efficiency at higher current densities, increased energy consumption at higher current densities, and energy consumption 1.2–2.0 fold higher for ROAW compared to AW.

Furthermore, it was found that even though sugars are neutral compounds, small amounts of lactose and galactose permeated into the ED concentrates. No glucose was detected in the ED concentrates except for AW ULCD despite the glucose concentration decreased in the diluates. Overall, it can be concluded that RO pre-processing of AW will be beneficial even though it results in longer processing times and higher energy consumptions, since the ROAW has a higher dry matter compared to AW. The main drawback of starting the process at OLCD is the associated highest energy consumption. However, the shortened processing time and increased lactate separation efficiency might be beneficial in specific cases, in which the processing time is a limiting factor.

Declaration of Competing Interest

The authors declare that they have no known competing financial interests or personal relationships that could have appeared to influence the work reported in this paper.

Acknowledgement

The authors would like to thank the staff of Hobro dairy for collection of acid whey. The present study is a part of the Platform for Novel Gentle Processing supported by the Dairy Rationalisation Fund (DDRF), Copenhagen University and Arla Foods.

Appendix A. Supporting information

Supplementary data associated with this article can be found in the online version at doi:10.1016/j.fbp.2023.05.002.

References

Andreeva, M.A., Gil, V.V., Pismenskaya, N.D., Dammak, L., Kononenko, N.A., Larchet, C., Grande, D., Nikonenko, V.V., 2018. Mitigation of membrane scaling in electrodialysis by electroconvection enhancement, pH adjustment and pulsed electric field application. J. Membr. Sci. 549, 129–140.

Atamanenko, I., Kryvoruchko, A., Yurlova, L., 2004. Study of the scaling process on membranes. Desalination 167, 327–334.

Beaulieu, M., Perreault, V., Mikhaylin, S., Bazinet, L., 2020. How overlimiting current condition influences lactic acid recovery and demineralization by electrodialysis with nanofiltration membrane: comparison with conventional electrodialysis. Membranes 10.

Beden, B., Largeaud, F., Kokoh, K.B., Lamy, C., 1996. Fourier transform infrared reflectance spectroscopic investigation of the electrocatalytic oxidation of d-glucose: identification of reactive intermediates and reation products. Electrochim. Acta 41, 701–709.

Carter, B., DiMarzo, L., Pranata, J., Barbano, D.M., Drake, M., 2021. Efficiency of removal of whey protein from sweet whey using polymeric microfiltration membranes. J. Dairy Sci. 104, 8630–8643.

Casademont, C., Farias, M., Pourcelly, G., Bazinet, L., 2008. Impact of electrodialytic parameters on cation migration kinetics and fouling nature of ion-exchange membranes during treatment of solutions with different magnesium/calcium ratios. J. Membr. Sci. 325, 570–579.

Chandra, A., Tadimeti, J.G.D., Bhuvanesh, E., Pathiwada, D., Chattopadhyay, S., 2018. Switching selectivity of carboxylic acids and associated physico-chemical changes with pH during electrodialysis of ternary mixtures. Sep. Purif. Technol. 193, 327–344.

Chandra, A., E, B., Chattopadhyay, S., 2022. A critical analysis on ion transport of organic acid mixture through an anion-exchange membrane during electrodialysis. Chem. Eng. Res. Des. 178, 13–24.

Chandrapala, J., Vasiljevic, T., 2017. Properties of spray dried lactose powders influenced by presence of lactic acid and calcium. J. Food Eng. 198, 63–71.

Chandrapala, J., Chen, G.Q., Kezia, K., Bowman, E.G., Vasiljevic, T., Kentish, S.E., 2016a. Removal of lactate from acid whey using nanofiltration. J. Food Eng. 177, 59–64.

Chandrapala, J., Wijayasinghe, R., Vasiljevic, T., 2016b. Lactose crystallization as affected by presence of lactic acid and calcium in model lactose systems. J. Food Eng. 178, 181–189.

Chen, A., Hansen, T.H., Olsen, L.I., Palmgren, M., Husted, S., Schjoerring, J.K., Persson, D.P., 2020. Towards single-cell ionomics: a novel micro-scaled method for multi-element analysis of nanogram-sized biological samples. Plant Methods 16, 31.

Chen, G.Q., Eschbach, F.I.I., Weeks, M., Gras, S.L., Kentish, S.E., 2016. Removal of lactic acid from acid whey using electrodialysis. Sep. Purif. Technol. 158, 230–237.

Christiansen, M.V., Dave, A., Skibsted, L.H., Ahrné, L., 2022. Functional properties of skim milk concentrates produced by reverse osmosis filtration and reconstituted commercial powders. Int. Dairy J. 126.

Cifuentes-Araya, N., Pourcelly, G., Bazinet, L., 2011. Impact of pulsed electric field on electrodialysis process performance and membrane fouling during consecutive demineralization of a model salt solution containing a high magnesium/calcium ratio. J. Colloid Interface Sci. 361, 79–89.

Cifuentes-Araya, N., Pourcelly, G., Bazinet, L., 2012. Multistep mineral fouling growth on a cation-exchange membrane ruled by gradual sieving effects of magnesium and carbonate ions and its delay by pulsed modes of electrodialysis. J. Colloid Interface Sci. 372, 217–230.

Cifuentes-Araya, N., Pourcelly, G., Bazinet, L., 2013. Water splitting proton-barriers for mineral membrane fouling control and their optimization by accurate pulsed modes of electrodialysis. J. Membr. Sci. 447, 433–441.

Cifuentes-Araya, N., Astudillo-Castro, C., Bazinet, L., 2014. Mechanisms of mineral membrane fouling growth modulated by pulsed modes of current during electrodialysis: evidences of water splitting implications in the appearance of the amorphous phases of magnesium hydroxide and calcium carbonate. J. Colloid Interface Sci. 426, 221–234.

Cowan, D.A., Brown, J.H., 1959. Effect of turbulence on limiting current in electrodialysis cells. Ind. Eng. Chem. 51, 1445–1448.

Dufton, G., Mikhaylin, S., Gaaloul, S., Bazinet, L., 2018. How electrodialysis configuration influences acid whey deacidification and membrane scaling. J. Dairy Sci. 101, 7833–7850.
Dufton, G., Mikhaylin, S., Gaaloul, S., Bazinet, L., 2019. Positive impact of pulsed electric field on lactic acid removal, demineralization and membrane scaling during acid whey electrodialysis. Int. J. Mol. Sci. 20.
Dufton, G., Mikhaylin, S., Gaaloul, S., Bazinet, L., 2020. Systematic study of the impact of pulsed electric field parameters (Pulse/Pause Duration and Frequency) on ED performances during acid whey treatment. Membranes 10.
Ganju, S., Gogate, P.R., 2017. A review on approaches for efficient recovery of whey proteins from dairy industry effluents. J. Food Eng. 215, 84–96.
Garcia, A.C., Vavrusova, M., Skibsted, L.H., 2018. Supersaturation of calcium citrate as a mechanism behind enhanced availability of calcium phosphates by presence of citrate. Food Res. Int. 107, 195–205.
Ghalloussi, R., Garcia-Vasquez, W., Chaabane, L., Dammak, L., Larchet, C., Deabate, S.V., Nevakshenova, E., Nikonenko, V., Grande, D., 2013. Ageing of ion-exchange membranes in electrodialysis: a structural and physicochemical investigation. J. Membr. Sci. 436, 68–78.
Guo, H., Xiao, L., Yu, S., Yang, H., Hu, J., Liu, G., Tang, Y., 2014. Analysis of anion exchange membrane fouling mechanism caused by anion polyacrylamide in electrodialysis. Desalination 346, 46–53.
Kim, Y., Walker, W.S., Lawler, D.F., 2012. Competitive separation of di- vs. mono-valent cations in electrodialysis: effects of the boundary layer properties. Water Res. 46, 2042–2056.
Lee, J.-W., Trinh, L.T.P., Lee, H.-J., 2014. Removal of inhibitors from a hydrolysate of lignocellulosic biomass using electrodialysis. Sep. Purif. Technol. 122, 242–247.
Lemay, N., Mikhaylin, S., Bazinet, L., 2019. Voltage spike and electroconvective vortices generation during electrodialysis under pulsed electric field: impact on demineralization process efficiency and energy consumption. Innov. Food Sci. Emerg. Technol. 52, 221–231.
Lemay, N., Mikhaylin, S., Mareev, S., Pismenskaya, N., Nikonenko, V., Bazinet, L., 2020. How demineralization duration by electrodialysis under high frequency pulsed electric field can be the same as in continuous current condition and that for better performances? J. Membr. Sci. 603, 117878.
Li, F., Guo, Y., Wang, S., 2022. Pilot-scale selective electrodialysis for the separation of chloride and sulphate from high-salinity wastewater. Membranes 12. https://doi.org/10.3390/membranes12060610
Lindstrand, V., Sundström, G., Jönsson, A.-S., 2000. Fouling of electrodialysis membranes by organic substances. Desalination 128, 91–102.
Menchik, P., Zuber, T., Zuber, A., Moraru, C.I., 2019. Short communication: composition of coproduct streams from dairy processing: acid whey and milk permeate. J. Dairy Sci. 102, 3978–3984.
Merkel, A., Ashrafi, A.M., 2019. An investigation on the application of pulsed electrodialysis reversal in whey desalination. Int. J. Mol. Sci. 20.
Merkel, A., Voropaeva, D., Ondrusek, M., 2021. The impact of integrated nanofiltration and electrodialytic processes on the chemical composition of sweet and acid whey streams. J. Food Eng. 298.
Mikhaylin, S., Bazinet, L., 2016. Fouling on ion-exchange membranes: classification, characterization and strategies of prevention and control. Adv. Colloid Interface Sci. 229, 34–56.
Mikhaylin, S., Nikonenko, V., Pourcelly, G., Bazinet, L., 2014. Intensification of demineralization process and decrease in scaling by application of pulsed electric field with short pulse/pause conditions. J. Membr. Sci. 468 (2014), 389–399.
Mikhaylin, S., Nikonenko, V., Pismenskaya, N., Pourcelly, G., Choi, S., Kwon, H.J., Han, J., Bazinet, L., 2016. How physico-chemical and surface properties of cation-exchange membrane affect membrane scaling and electroconvective vortices: influence on performance of electrodialysis with pulsed electric field. Desalination 393, 102–114.
Nielsen, E.N., Merkel, A., Yazdi, S.R., Ahrné, L., 2021. The effect of acid whey composition on the removal of calcium and lactate during electrodialysis. Int. Dairy J. 117.
Nielsen, E.N., Skibsted, L.H., Yazdi, S.R., Merkel, A., Ahrné, L.M., 2022a. Effect of calcium-binding compounds in acid whey on calcium removal during electrodialysis. Food Bioprod. Process. 131, 224–234.
Nielsen, E.N., Skibsted, L.H., Yazdi, S.R., Merkel, A., Ahrné, L.M., 2022b. Improving electrodialysis separation efficiency of minerals from acid whey by nano-filtration pre-processing. Int. J. Dairy Technol. 75, 820–830.
Nielsen, E.N., Cordin, U., Gøtke, M., Velizarov, S., Galinha, C.F., Skibsted, L.H., Crespo, J.G., Ahrné, L.M., 2023. Fouling of ion-exchange membranes during electrodialytic acid whey processing analysed by 2D fluorescence and FTIR spectroscopy. Sep. Purif. Technol. 316, 123814.
Pasta, M., Mantia, La, Cui, Y, F., 2010. Mechanism of glucose electrochemical oxidation on gold surface. Electrochim. Acta 55, 5561–5568.
Pismenskaya, N., Laktionov, E., Nikonenko, V., El Attar, A., Auclair, B., Pourcelly, G., 2001. Dependence of composition of anion-exchange membranes and their electrical conductivity on concentration of sodium salts of carbonic and phosphoric acids. J. Membr. Sci. 181 (2), 185–197.
Pismenskaya, N., Nikonenko, V., Volodina, E., Pourcelly, G., 2002. Electrotransport of weak-acid anions through anion-exchange membranes. Desalination 147, 345–350.
Rasmussen, P.K., Suwal, S., van den Berg, F.W.J., Yazdi, S.R., Ahrné, L., 2020. Valorization of side-streams from lactose-free milk production by electrodialysis. Innov. Food Sci. Emerg. Technol. 62.
Rybalkina, O.A., Sharafan, M.V., Nikonenko, V.V., Pismenskaya, N.D., 2022. Two mechanisms of H+/OH– ion generation in anion-exchange membrane systems with polybasic acid salt solutions. J. Membr. Sci.
Shaposhnik, V.A., Zubets, N.N., Strygina, I.P., Mill, B.E., 2002. High demineralization of drinking water by electrodialysis without scaling on the membranes. Desalination 145 (1–3), 329–332.
Suárez, A., Riera, F.A., 2015. Production of high-quality water by reverse osmosis of milk dairy condensates. J. Ind. Eng. Chem. 21, 1340–1349.
Syrios, A., Faka, M., Grandison, A.S., Lewis, M.J., 2011. A comparison of reverse osmosis nanofiltration and ultrafiltration as concentration processes for skim milk prior to drying. Int. J. Dairy Technol. 64, 467–472.
Talebi, S., Suarez, F., Chen, G.Q., Chen, X., Bathurst, K., Kentish, S.E., 2020. Pilot study on the removal of lactic acid and minerals from acid whey using membrane technology. ACS Sustain. Chem. Eng. 8, 2742–2752.
Zabolotskii, V.I., Shel'deshov, N.V., Gnusin, N.P., 1988. Dissociation of water molecules in systems with ion-exchange membranes. Rus. Chem. Rev. 57, 8.